Chapter 13

High-Quality Carbon Nanomaterials Synthesized by Excimer Laser Ablation

Calin-Constantin Moise and Marius Enachescu

Additional information is available at the end of the chapter

http://dx.doi.org/10.5772/65309

Abstract

Due to their special physical and chemical properties and potential applications from hydrogen storage to medical implantation, the carbon-based nanomaterials are in the frame of attention for many research groups all over the world. As synthesis techniques, we highlight arc discharge, chemical vapor deposition (CVD) and laser ablation. Even an expensive technique, laser ablation is suitable for single-wall carbon nanotubes (SWCNTs) synthesis, providing the highest yield of over 70%, while arc discharge yield is about 30% and CVD is about 42%. The most common investigation methods for carbon nanomaterials are micro-Raman spectroscopy, thermo-gravimetric analysis (TGA) and morphological and topographic studies done by atomic force microscopy (AFM), scanning electron microscopy (SEM), transmission electron microscopy (TEM) and high-resolution transmission electron microscopy (HR-TEM). We also emphasize in this work that by involving a home-designed reactor, we successfully synthesized SWCNTs, carbon nano-onions (CNOs) as well as graphene in the same reactor. Tuning the experimental parameters, we switch the end type of nanomaterials. We have done comprehensive studies regarding the carbon nanomaterials synthesis.

Keywords: laser ablation, SWCNTs, carbon nano-onions (CNOs), graphene, AFM, SEM, TEM, STEM, HR-TEM, HR-STEM, EDX, micro-Raman spectroscopy

1. Introduction

1.1. Short history of carbon nanomaterials

During the last three decades multiple types of carbon nanomaterials were discovered: fullerenes in 1985 (Nobel Prize 1996) [1], carbon nanotubes (CNTs) in 1991 [2], followed by

single-wall carbon nanotubes (SWCNTs) in 1993 [3] and graphene in 2007 (Nobel Prize 2010) [4]. Due to their physical and chemical properties, carbon nanomaterial applications cover a wide range, from hydrogen storage to medical implantation.

1.2. Physical properties of carbon nanotubes

Figure 1 illustrates the comparison of SWCNTs properties against all known materials. For instance, the electrical conductivity is 1000 times higher than cooper, Young modulus almost same as diamond, tensile strength up to 14 times higher than Kevlar and thermal conductivity almost same as aluminum.

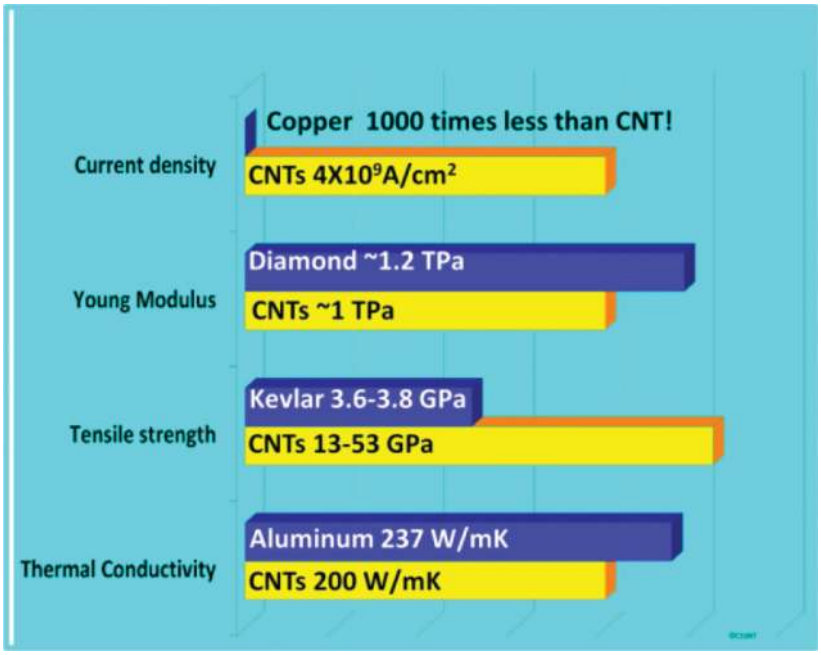

Figure 1. Properties of SWCNTs versus known materials.

1.3. Potential applications of carbon nanomaterials

In **Figure 2**, we select some of the potential applications for SWCNTs. One of the interesting application of SWCNTs is hydrogen storage. SWCNTs have high surface area; curvature creates cavities of molecular dimensions and superpositions of potential fields in cavities lead to large attractive force on hydrogen molecules [5]. SWCNTs are capable of adsorbing hydrogen quickly, to high density, at ambient temperatures and pressures [6–8]. The SWCNTs have been used in different types of applications such as biosensors [9], chemical sensors [10], scanning microscope tips [11], nanoelectronics [12], and third generation solar cell [13].

http://dx.doi.org/10.5772/65309

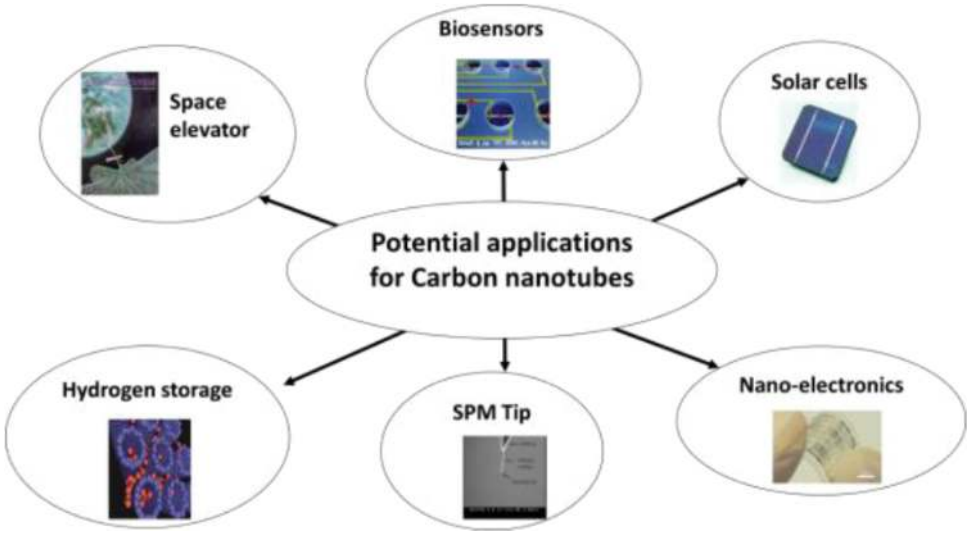

Figure 2. Potential applications of SWCNTs.

1.4. The routes for synthesis of carbon nanomaterials

There are several methods employed to obtain carbon nanomaterials. They are described very well by Tomanek in [14].

The nanotubes synthesis involve high energetic or temperature processes such as: arc evaporation (AE), chemical vapor deposition (CVD), conversion of carbon monoxide at high pressure in HiPCO process, ball milling (BM), as well as, the pulsed laser vaporization (PLV).

Arc discharge or arc evaporation (AE) can be used successfully for fullerenes, multi-wall carbon nanotubes and single-wall carbon nanotubes synthesis. Direct current of 10-20V is supplied to electrodes in a cooling inert gas environment. Nanotubes are formed on cathode during electrode evaporation in the direction of electric field lines. On the other hand fullerenes are founded in the soot on chamber walls. For syntheses of single-wall nanotubes the presence of catalyst into electrodes is required [2, 15].

The chemical vapor deposition (CVD) is a very common process for covert hydrocarbons gases into a diamond-like carbon (DLC) coating or carbon nanotubes. Conversion takes place at high temperature in thermal CVD, or can be assisted by plasma in plasma-enhanced CVD (PE-CVD). In the presence of water and by using a substrate (usually silicon) vertically aligned nanotube arrays (VANTAs) can be obtained by CVD. This process is called "Supergrowth".

A low-cost synthesis technique for nanotubes and related nanostructures from layered substances, such as graphite is the ball milling (BM). The BM is performed at room temperature, but the impact of a macroscopic ball on a powdered substance leads locally to a temperature increase that enables rearrangement of chemical bonds. Changes are induced in chemical

bonding and structure by pressure, often introduced by hitting the material with a foreign object.

Pulsed laser vaporization (PLV) or laser ablation is a technique to produce high-quality carbon nanostructures. A laser beam is focused on a heated carbon target. The resulting plume and vapors are carried by an inert gas to a cooled cooper collector called cold finger (CF), where the raw material condenses. A sea urchin, also known as a dahlia structure, is a colloquial designation for the compact agglomeration of carbon nano-horns formed during the laser ablation process.

PLV or PLD (pulsed laser deposition) is the technique that will be in great detail described below along the results of the synthesis obtained using this method.

2. Laser ablation

We will focused in this section on synthesis of SWCNTs and other carbon nanomaterials via laser ablation since this is the technique used in ours laboratories. The pulsed laser ablation process for production of SWCNTs has first been reported by Guo *et al.* [16]. Nanotubes produced by laser ablation are up to 90% pure [17]. The target consists of mainly graphite to which small amounts of metal catalysts are added.

The laser ablation takes place inside a quartz tube heated to 800–1200°C [16, 18, 19] through which an ablation gas is used to control the dynamics of the plume and carry the ablation products to a cooled collector. Among the gases investigated Argon has been the most studied [16, 18, 19], but we and others proved that other gases like nitrogen [20, 21], krypton [20, 22], neon [20, 23], and helium [24] are also suitable for SWCNTs production by laser ablation.

2.1. Different types of reactors for laser ablation experiments

Previous laser ablation experiments have been focused on a chamber design commonly referred to as "front pumped counter flow pulse laser vaporization (PLV)". The design, presented in **Figure 3(a)** consists of an electric oven having a quartz tube inserted into it. The carbon target doped with small amount of metal catalyst (1) is located in the mid-position inside the quartz tube. The laser beam passes a quartz window (3) and is focused on the target. The ablation gas is fed from the front of reactor and a vacuum pump is located downstream of the cold finger (2) generating an even flow and pressure inside of the tube. The plume resulting from ablation of the target and evaporated species are transported by the inert gas toward the cold finger where they condense. Guo *et al.* reported for the first time SWCNTs production by laser ablation using a typically front pumped counter flow PLV [16].

Some other experiments have been carried out using a similar chamber design [18, 19].

Another chamber design includes a smaller quartz tube through which the carrier gas can be fed close to the target in order to confine the plume to a smaller region [17, 25].

http://dx.doi.org/10.5772/65309

In **Figure 3(b)**, the schematically design is represented. These simple designs proved to be effective.

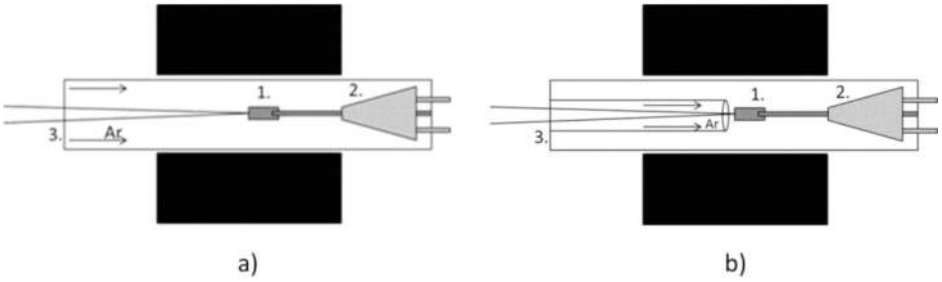

Figure 3. (a) Design of front pumped counter flow PLV system [16, 18, 19]; (b) design of front pumped counter flow PLV system with inner tube [17, 25].

The short length of the oven is the main disadvantage of these designs. From here is resulting a small zone were the ablation medium could be maintained at a certain needed temperature. Short oven is equivalent with a high temperature gradient into the ablation chamber. In our new design this disadvantage is avoided.

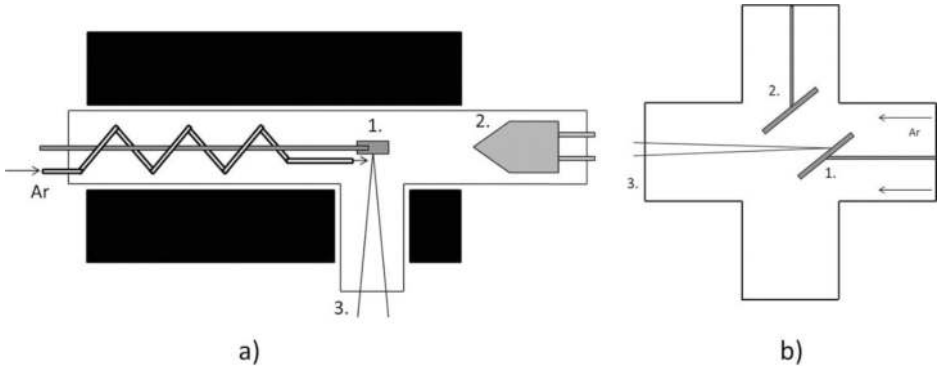

Figure 4. (a) Design of "T"-shaped PLV chamber with laser entrance from the side [26]; (b) "X"-shaped PLV chamber [27].

For increasing the ablated surface Holloway *et al.* proposed A "T" shaped quartz tube where the laser enters the chamber from the side [26]. The design is schematically represented in **Figure 4(a)**. The design includes feeding the ablation gas through a narrow tube coiled around the transfer rod in order to obtain a higher surface, thus increasing the heat transfer. The narrow tube takes the hot gas close to the target so that the products are carried away towards the cold finger. By this method can be ablated a bigger surface of the target. Complexity of the system which implies a custom made quartz tube with a side viewport for laser is the main disad-

vantage of this design. Geometry of the oven providing heating and temperature into the chamber is changed by this design.

The geometry becoming cumbersome and harder to control, resulting in high temperature gradients and a turbulent flow of the gas.

A chamber in "X" shape similar to those used for thin film depositions was proposed by Yahya *et al.* [27]. In **Figure 4(b)** is shown this design. The target (1) is positioned at an angle (usually 45°) parallel with water cooled substrate (2) at different distances. A quartz tube is not needed for this design, only the laser entrance window resulting in a more robust and easy to fabricate system. The system is usefully since it can be used for other purposes such as film deposition. With this type of reactor only multi walled carbon nanotubes (MWCNTs) were obtained. The system is not heated into an oven making impossible for the plume to reach eutectic point. May be this is one of the reasons that SWCNTs have not been obtained using such a chamber design. Other disadvantage of such reactor is the inert gas is not directed to carry the products from target to substrate, but only provides an inert atmosphere inside.

2.2. Our new chamber design

Figure 5 presents a cut-away side view of the novel experimental set-up developed and used in our research for the laser ablation of the targets [28]. The laser ablation chamber consists of a quartz tube, 50 mm in diameter and 1260 mm long, inserted into an oven. The quartz tube is O-ring sealed and operates from 10^{-3} Torr up to atmospheric pressure and temperature is controlled from 30 to 1200°C.

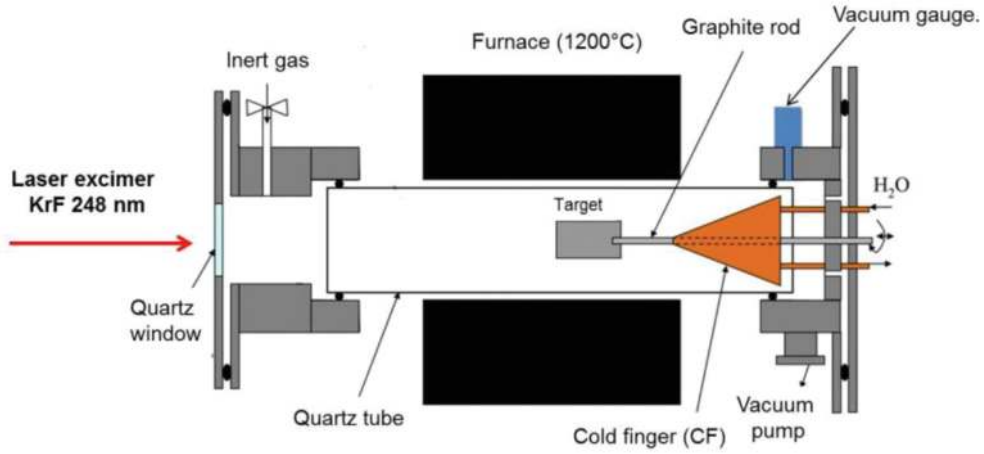

Figure 5. New reactor – Patent pending.

Laser ablation starts by passing the laser beam through a UV transparent quartz window and enters into the quartz tube hitting the target, when the target material begins to be ablated. The

http://dx.doi.org/10.5772/65309

target having 20 mm in diameter is mounted on a graphite rod. Target was rotated during ablation with constant speed to get uniform ablation. Then the inert gas, which enters from the left-up side of the reaction chamber, moves through the quartz tube to the heated area, e.g., at 1100°C, where the reaction takes place, transporting the ablation product toward a copper condenser called cold finger (CF), where it will be deposited as black soot. The cold finger was cooled to 12°C using water supplied by a chiller. The inert atmosphere and the transportation of the ablated material to the CF were maintained by using the carrier gas at a certain flow rate, e.g., 70 L/h. The pressure is maintained by pumping through a needle valve and measured by a vacuum gauge sitting just outside the chamber.

The KrF excimer laser used for the ablation is a Coherent COMPex Pro 205 equipment, having the wavelength of 248 nm and the pulse duration of 20 ns.

Our system has some special technical features:

(i) The length of the oven was doubled compared with previous designs [16, 29], to ensure a more uniform temperature in the ablation reactor, allowing the product to travel longer time in the constant heated zone favoring the growth of the SWCNTs.

Figure 6(a) shows a schematic comparison between size accurate representations of our chamber design and other chamber designs [16, 18, 19]. Ratio of the length of the new chamber versus older designs is over 2:1. The temperature distribution expected as a result of increased oven length is represented by the red semicircles. Kataura *et al.* have shown that increasing the furnace temperature and the time spent by the ablation products at this elevated temperature increases the SWCNTs production yield [30].

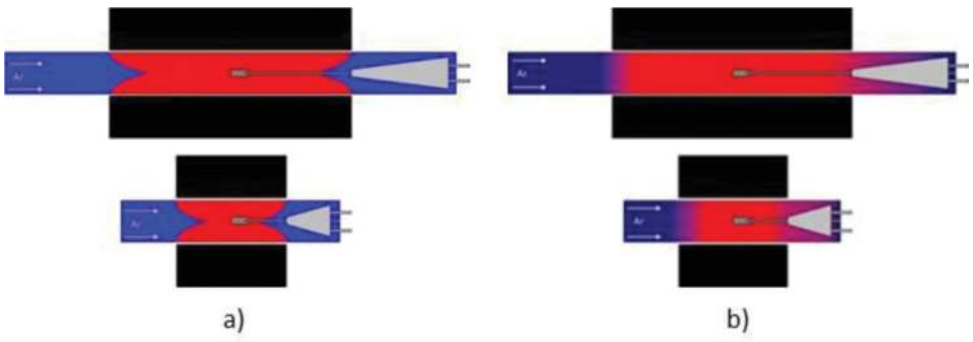

Figure 6. Our design (above) [28] and previously used chamber designs (below) [16, 18, 19]: (a) schematic representation of the heated area inside the ablation chamber; (b). Schematic representation of temperature gradient given by the water cooled cold finger. Ratio of the length of the new cold finger versus older design is 4.5:1.

(ii) The cold finger is longer (260 mm) with a larger surface than the previous one [28, 31], increasing the temperature gradient over its length and improving the capture of the product. A comparison of them is displayed in **Figure 7**, from where we can see that ratio of the length of the new cold finger versus older designs is over 4.5:1.

Figure 7. Photograph of the new and previous designed cold fingers.

The longer cold finger provides a larger surface resulting in a better percentage collection of the ablation products. The temperature gradient induced by the collector outside the oven area is distributed on a larger length of the cold finger, as presented in **Figure 6(b)**. This provides the means to study the influence the cold finger temperature gradient has on the condensation of the ablation products, i.e., the final products.

(iii) The attached Alicat flow meter controller allows controlling accurately the flow rate of the carrier gas over a wide range, 0–10 normal liters per minute (NLPM), with a resolution of 0.01 NLPM.

2.3. Original target preparation method

The target was prepared by following a recipe developed by Enachescu's group [28, 31, 32]. This recipe involves the mixing of graphite cement (GC 8010-B from Metal Forming Lubricants) with metal catalysts powder (Sigma Aldrich). We have studied several target compositions using uni- as well as bi-components metal catalysts. From all the combinations the best composition for SWCNTs synthesis was found to be Co 0.6%, Ni 0.6%, and C 98.8% (atomic percentage).

The mixture was transferred into a Teflon mold (20 mm diameter) and then cured 4 h at 130°C in air to increase the mechanical strength. Further another heat treatment of the target was applied for 1 h at 800°C in inert atmosphere to remove all the remaining organic compounds.

Material type	Pressure (Torr)	*T* (°C)	*E* (mJ)	RR (Hz)	Flow L/h	Catalyst
SWCNTs	500	1100	650	30	70	yes
CNOs	7	900	700	10	300	no
Graphene	100	1100	700	30	300	no

Table 1. The parameters used for carbon nanomaterial synthesis.

http://dx.doi.org/10.5772/65309

2.4. Recipes for carbon nanomaterial synthesis

We successfully synthesized SWCNTs, carbon nano-onions (CNOs) as well as graphene in the same reactor. Tuning the experimental parameters we switch the end type of nanomaterial. **Table 1** shows the parameters used for carbon nanomaterial synthesis. For SWCNTs synthesis, target must contain metallic catalyst grains. The parameters in the table are pressure in reaction chamber during ablation, oven temperature, laser pulse energy, repetition rate of laser pulses and the flow of inert gas.

3. Characterization experiments for SWCNTs

In previous work [28, 32], we found the suitable parameters for SWCNTs production:

- target composition Co 0.6%, Ni 0.6%, and C 98.8% (atomic percentage);

- oven temperature 1100°C;

- repetition rate of laser pulses 30 Hz;

- inert carrier gas pressure 500 Torr.

In the next subchapters we present the characterisation of SWCNTs obtained under above described conditions.

3.1. Micro-Raman spectroscopy experiments

Micro-Raman spectroscopy is a great investigation tool for SWCNTs characterization. In **Figure 8**, is a comparison of the typical micro-Raman spectra for SWCNTs obtained in our laboratories (blue) and high-quality commercially one (black), provided by Sigma Aldrich. As can be observed the spectra are quite similar leading to the conclusion that quality of SWCNTs obtained in our laboratory is comparable to commercial one.

The excitation laser was green (532 nm). In the zone of radial breathing mode (RBM) in **Figure 8** left top we found peaks characteristic only to SWCNTs and whose frequencies are strongly SWCNTs diameter dependent. The diameters were calculated in accordance with Eq. (1):

ω – frequency for vibrations in the radial direction [cm^{-1}];

$c1$, $c2$ – constants [cm^{-1}]; $c1 = 215$ [cm^{-1}]; $c2 = 18$ [cm^{-1}];

d – diameter of the nanotube [nm].

$$d = \frac{c1}{\omega - c2} \tag{1}$$

The diameters of our SWCNTs are in the range of $d = 1.1–1.6$ nm with average $d_A = 1.35$ nm.

The G band in the Raman spectra clearly demonstrates, depending on the ratio of I_{G+}/I_{G-} that semiconducting SWCNTs were obtained, **Figure 8** (top right). However by using red excitation laser we obtain evidence of metallic SWCNTs existence (not shown here). So we conclude that our material is a mixture of semiconducting and metallic nanotubes.

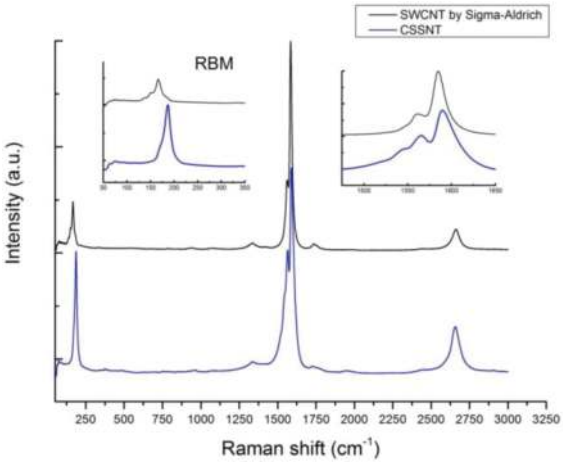

Figure 8. Micro-Raman spectra of SWCNTs – blue: our product, black: commercial product.

3.2. AFM experiments

Atomic force microscopy (AFM) was involved for the synthesized SWCNTs characterization as well as for SWCNTs mixed with poly(3-octylthiophene) (P3OT) polymer, for solar cell applications.

In **Figure 9** we present AFM images for a synthesized SWCNTs bundle on Si substrate: (a) 2D and; (b) 3D. In (c) is presented the topography of P3OT polymer on glass and (d) is 12% SWCNTs composite in P3OT polymer on glass and we can observe the SWCNTs bundles. We investigated also the adhesions forces on both surface and they increase with the increase of SWCNTs content into polymer (not shown here).

3.3. SEM experiments

In **Figure 10** is a collection of images obtained by a field emission scanning electron microscopy (SEM) for synthesized SWCNTs. The high resolution of SEM system of 0.6 nm, is making possible direct visualization and direct measuring of the SWCNTs bundles into SEM images. Usually such measurements are performed in high resolution transmission electron microscopy (HR-TEM), where the sample preparation is laboriously comparing with SEM sample investigations. We can identify well defined nanotubes shapes with μm length and nm diameters and observe their abundance. It is very interesting to observe their parallel arrangement.

http://dx.doi.org/10.5772/65309

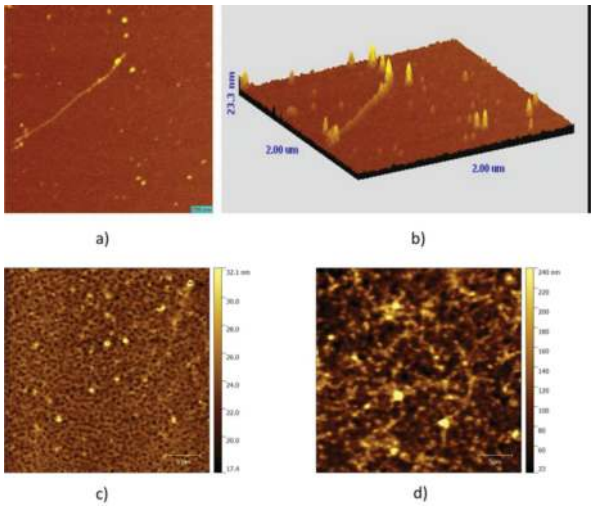

Figure 9. AFM images (a) 2D; (b) 3D; (c) 100% polymer; (d) 12% SWCNTs in polymer.

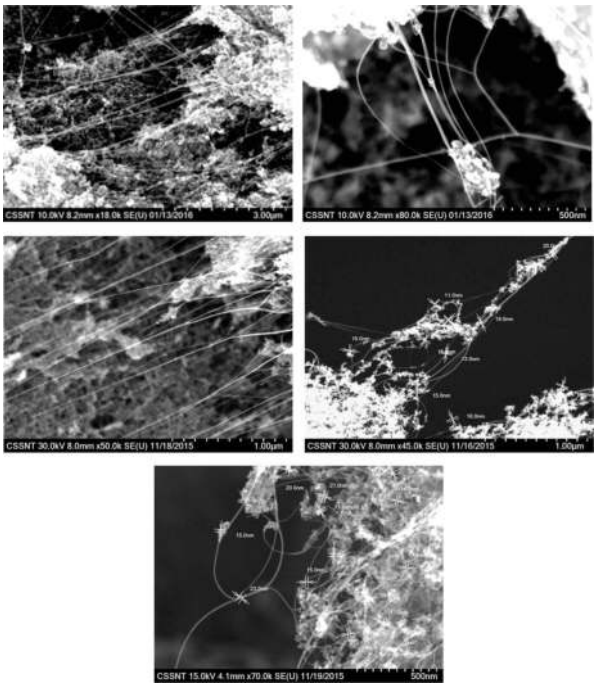

Figure 10. SEM images of synthesized SWCNTs.

3.4. SEM-Z contrast-STEM-EDX combined experiments

An advanced surface science system, capable of SEM and scanning transmission electron microscopy (STEM) investigations, performed at the same location of a specimen, was involved for the synthesized SWCNTs.

The special features of the synthesized SWCNTs are presented in **Figure 11** based on the capabilities of the special equipment presented above: *SWCNTs images in SEM, Z contrast (atomic mass contrast), STEM and energy dispersive X-ray spectroscopy (EDX) modes at the same sample location*. The images allow to a clear identification of catalysts grains and amorphous carbon (EDX mapping sustained also by Z contrast image) and in **Figure 11(d)** we observe that carbon is wide-spread. In SEM and STEM mode we can see the nanotubes shape and observe the opposite contrast of the images (a) and (c).

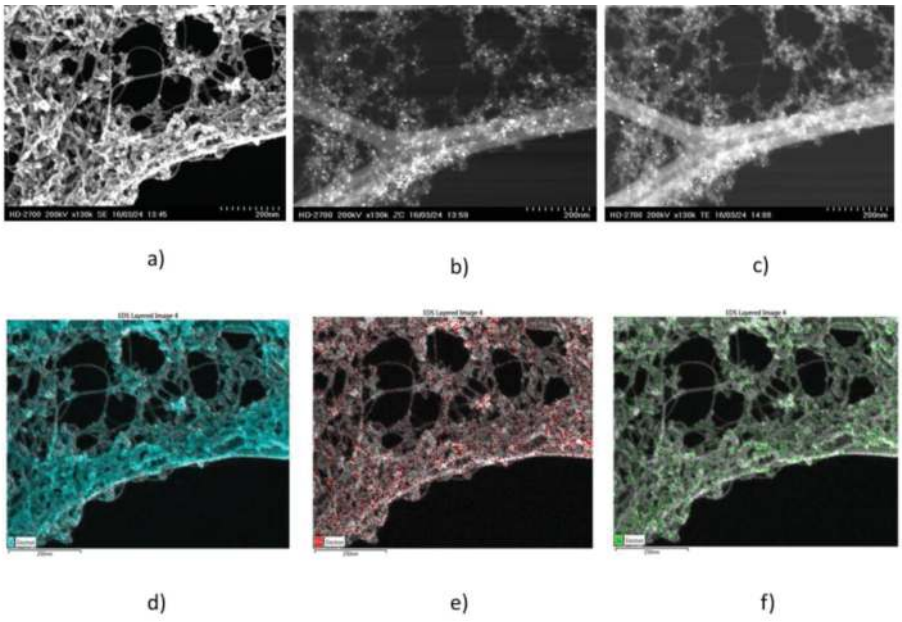

Figure 11. SWCNTs images taken at the same sample location in (a) SEM mode; (b) Z-contrast mode; (c) STEM mode; (d–f) EDX mapping mode for C, Co, Ni, respectively.

3.5. HR-STEM experiments

In order to get direct information on the morphology of the synthesized SWCNTs, we performed HR-STEM investigations.

We measured the diameters of several SWCNTs using HR-STEM images as in **Figure 12**. The measured diameters distribution and its histogram are plotted in **Figure 13(a)** and **(b)**, re-

http://dx.doi.org/10.5772/65309

spectively. The histogram of diameters distribution was in the range of 1.0–1.7 nm, and the center between 1.25 and 1.35 nm [23]. This result is in great agreement with the result obtained from micro-Raman measurements (average d_A = 1.35 nm).

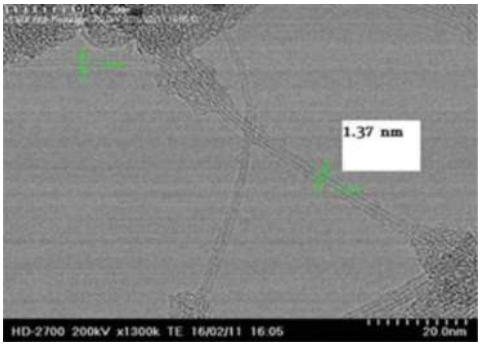

Figure 12. The measurement of SWCNTs diameter by HR-STEM.

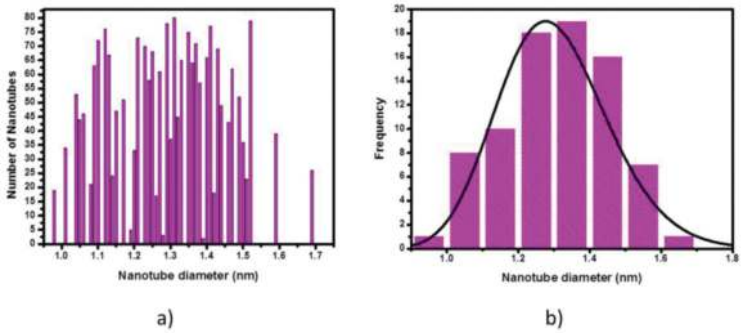

Figure 13. (a) Measured diameters distribution of SWCNTs. (b) Histograms of diameter distribution of the SWCNTs.

3.6. TGA experiments

Thermo-gravimetric analysis (TGA) was involved for the synthesized SWCNTs characterization as well as for the target composition used for obtaining the SWCNTs.

We analyzed by TGA, graphite powder, and materials used for our target. They burn in the same zone denoting that our target is graphitized. On the other hand collected material from cold finger (SWCNTs, green curve) burn in totally different place confirming it is a different material. What we also depicted in **Figure 14** is that ablation take place with respecting the target stoichiometry since the target materials and SWCNTs contain same percentage of remaining catalyst metals. From TGA curves we estimate a 70% yield of SWCNTs in raw product.

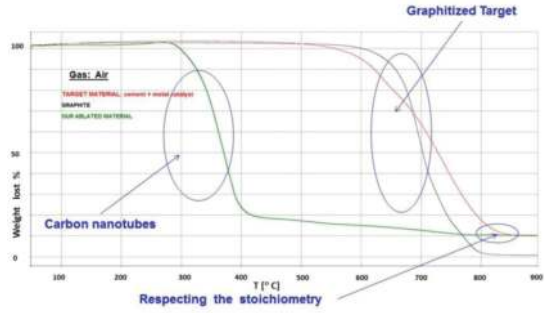

Figure 14. TGA curves for graphite powder (black), target material (red), SWCNTs (green).

3.7. Influence of carrier gas over SWCNTs synthesis

3.7.1. Experimental description

In an effort to compare our work with the work of Nishide *et al.* [20] which used Nd-YAG (neodymium-doped yttrium aluminium garnet; Nd:Y3Al5O12) laser, we study the SWCNTs synthesis versus different inert carrier gas used during the ablation with KrF excimer laser. For this study we varied the ablation gas types while the other parameters: laser type, laser energy, pulse repetition rate, oven temperature, gas pressure, gas flow rate, and ablation time remained constant (**Table 2**). The laser ablation experiments were carried out in four different inert gases: argon, nitrogen, neon, and helium.

Parameter	Value
Laser type	Excimer KrF, 248 nm
Laser energy	600 mJ
Repetition rate	30 Hz
Pulse period	20 ns
Oven temperature	1100°C
Gas pressure	500 Torr
Ablation time	60 min

Table 2. Parameters used for SWCNTs synthesis in different gas carrier environment.

3.7.2. Ablated mass and collected mass

We measured the mass of the target before and after ablation and also the raw product collected mass, i.e., SWCNTs. We observed linear decrease of ablated mass with the increase of carrier gas molecular mass. Also the collected mass follows the same trend, so we can increase and optimize the SWCNTs production by changing carrier gas. Fitting lines are shown in **Figure 15**.

http://dx.doi.org/10.5772/65309

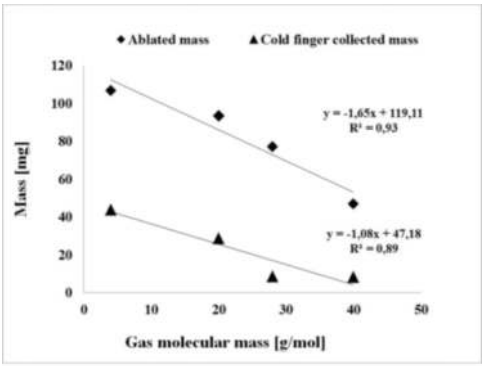

Figure 15. Ablated mass and collected mass versus gas molecular mass.

3.7.3. Micro-Raman experiments

Typical micro-Raman spectra for SWCNTs obtained in different inert gases are shown in **Figure 16(a)**. The excitation laser was green, 532nm.

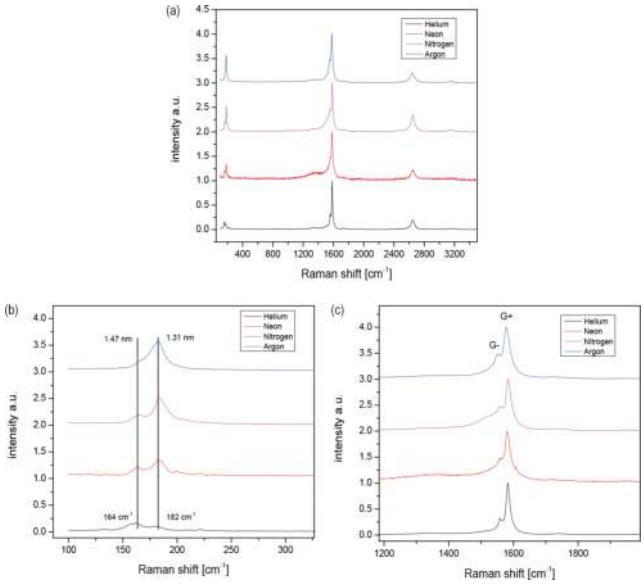

Figure 16. (a) Micro-Raman spectra for SWCNTs obtained using different ablation gases; (b) Radial breathing mode (RBM) part of the spectra; (c) G band part of the spectra.

In the zone of radial breathing mode (RBM) **Figure 16(b)** we found two peaks whose frequencies are strongly SWCNTs diameter dependent. The diameters were calculated in accordance

with Eq. (1). For all gases two diameters distribution of 1.31 and 1.47 nm were calculated see **Figure 16(b)** (black lines) in great agreement with the result obtained from statistically HR-STEM measurements 1.25–1.35 nm (**Figure 13**).

3.7.4. TGA experiments

As can be seen in **Figure 17** we found different yields of SWCNTs versus the gas carrier. In **Table 3** using the yields and collected mass we calculate the mass of SWCNTs contained in the soot and the highest value was obtained in helium, almost 10 times more than in argon.

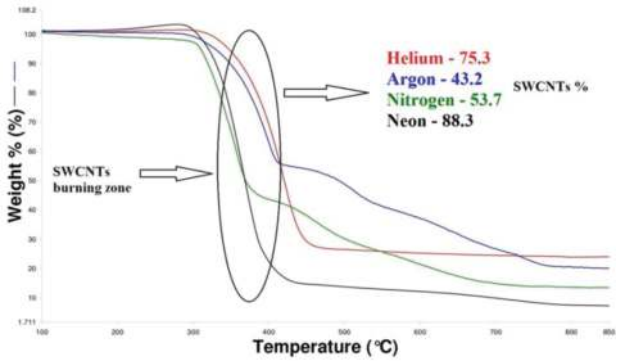

Figure 17. TGA curves of the ablation product, i.e., SWCNTs, obtained in different inert gases (Gas: air, T = 100–850°C).

Carrier gas	Mass of deposition onto cold finger [mg]	Percentage of SWCNTs in the deposition from TGA curves	Mass of SWCNTs produced [mg]
He	44	75.3	33.1
Ne	28.7	88.3	25.3
N_2	8.6	53.7	4.6
Ar	8.4	43.2	3.6

Table 3. SWCNTs mass calculated from the TGA curves.

4. Characterization experiments for CNOs

Under condition described in **Table 1** we obtain in our laboratories high quality CNOs [33].

4.1. Micro-Raman experiments

In **Figure 18** the induced defects and disorder are related to D band (1350 cm^{-1}), G band (1550–1620 cm^{-1}) represents vibrations in graphene plane and D' band (2500–3000 cm^{-1}) correspond to secondary order Raman scattering (second order of D and G bands).

http://dx.doi.org/10.5772/65309

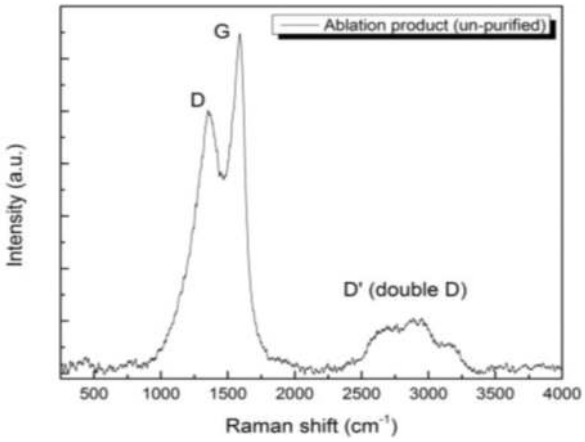

Figure 18. Raman band characteristics to CNOs.

The ratio of the D and G band intensity (I_D/I_G), which is related with the crystalline perfection was calculated and is 0.63. This value indicates that the CNOs synthesized by laser ablation shown a high crystallinity. Pimenta proposed an empirical formula (2) for determine in-plane crystallite size L_a in nm [34].

$$L_a = \frac{560}{E^4}\frac{I_G}{I_D} \tag{2}$$

where E is the excitation energy in eV (2.33 eV). Thus, resulting L_a value based on this formula is about 30 nm.

4.2. SEM experiments

As can be observed in **Figure 19** by ablating the target under conditions for CNOs we obtain totally different material comparing with SWCNTs images from **Figure 10**. The raw material looks as well defined spherical shapes.

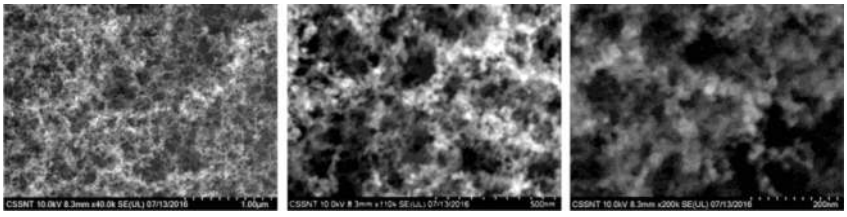

Figure 19. SEM images of CNOs.

4.3. HR-TEM experiments

The products obtained by ablating the pure graphite target using conditions for CNOs synthesis in **Table 1**, look like well-defined nano-onions, both individual and clustered through a matrix of amorphous carbon. As can be seen in **Figure 20(a)** the diameter is between 10 and 25 nm which is in good agreement with the dimensions obtained from micro-Raman spectroscopy using Pimenta formula (2).

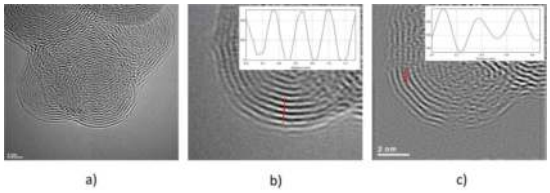

Figure 20. (a) CNOs clustered; (b) CNOs profile perpendicular to shells (c) CNOs profile along of the shell.

If we measure the graphitic interlayer distance of the CNOs from perpendicular direction to shells profile we found 0.35 nm in great agreement with the graphene monolayer thickness (**Figure 20(b)**). On the other hand if we analyze the profile in along of shell we found the distance between two consecutive atoms to be 0.24 nm, in good agreement with the atomic lattice on graphene **Figure 20(c)**.

4.4. TGA experiments

In order to measure the purity of obtained CNOs we perform thermo-gravimetric analysis (TGA) as can be seen in **Figure 21**. The percentage of weight lost has been measured using a constant heating rate of 5°C/min under a 20 mL/min Ar flux that limited the oxygen content in the furnace.

The mass loss between 350 and 600°C was assigned to the oxidation of the CNOs and is about 94%.

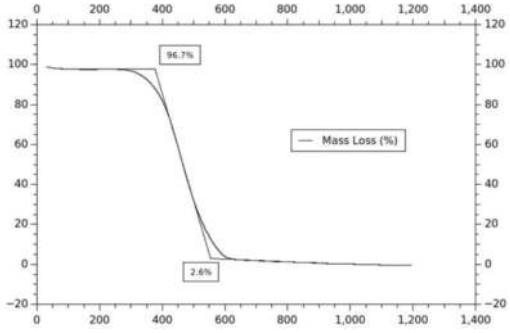

Figure 21. TGA curves of the CNOs (Gas: argon, T = 50–1200°C).

http://dx.doi.org/10.5772/65309

5. Characterization experiments for graphene

The products obtained by ablating the pure graphite target under condition for graphene in **Table 1**, look like well-defined graphene sheets.

5.1. SEM experiments

High quality graphene sheets obtained by laser ablation in our reactor are shown in **Figure 22**. As can be seen the amorphous carbon content is small. We observe in **Figure 22** that by ablating the target under conditions for graphene product we obtain totally different material comparing with SWCNTs images from **Figure 10** and CNOs images from **Figure 19**.

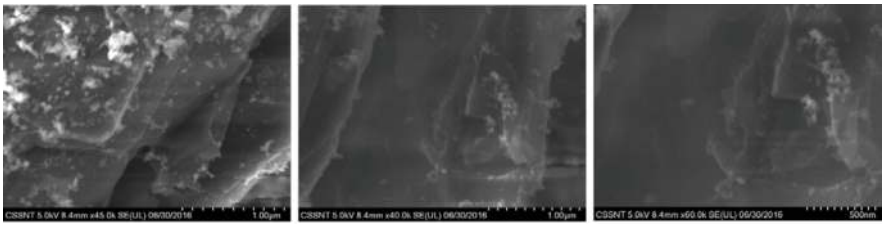

Figure 22. SEM images of graphene sheets.

5.2. TEM and electron diffraction experiments

In **Figure 23** we can observe nice transparent graphene flakes obtained in our reactor. The electron diffraction pattern is confirming the presence of graphene (nicely hexagonally concentric shapes).

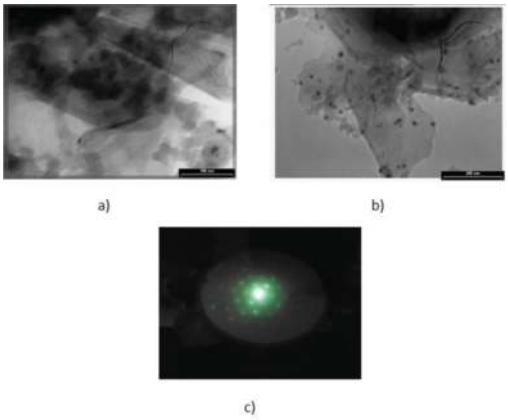

Figure 23. Graphene TEM images: (a) and (b) graphene sheets; (c) electron diffraction pattern.

5.3. SEM-Z contrast-STEM combined experiments

The special features of the synthesized graphene are presented in **Figure 24** based on the capabilities of the special equipment presented above: *graphene images in SEM mode, Z contrast and STEM modes at the same sample location*. In these amazing images the SEM mode image suggest two graphene sheets one top of the other. This is confirmed by STEM image, since the top part is black denoting thicker structure. On the other hand the Z contrast image is showing only the presence of carbon in the sample. *This is one of the great advantages to have images in different modes on the same sample location*.

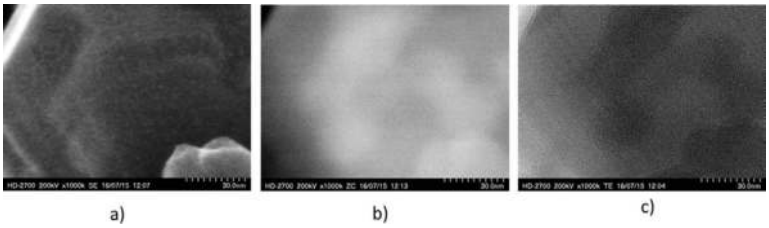

Figure 24. Graphene images in (a) SEM mode; (b) Z-contrast mode; (c) STEM mode.

5.4. HR-STEM experiments

Figure 25(a) is a very good quality HR-STEM image of graphene sheet. We can observe the carbon atoms and their periodically disposal into lattice. Also we performed fast Fourier transform (FFT) and as can be seen in **Figure 25(b)** we identified two directions with crystalline planes.

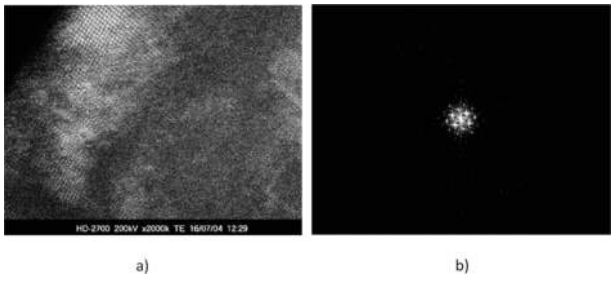

Figure 25. Graphene: (a) HR-STEM image (b) FFT image.

5.5. Nano-diffraction experiments

To confirm the presence of graphene in our product we performed electron nano-diffraction measurement. We can see in **Figure 26** that the diffraction pattern is confirming the presence of graphene (nicely hexagonally shape).

http://dx.doi.org/10.5772/65309

Figure 26. Nano-diffraction experiment on graphene.

6. Conclusion

The present work highlighted the important specific synthesis way of carbon based nanomaterials, especially SWCNTs, and described the most used production routes using laser ablation technique.

We proved by micro-Raman spectroscopy, AFM, SEM, TEM, HR-TEM, STEM, HR-STEM, SEM-STEM, and TGA that high quality of carbon nanomaterials have been synthesized via laser ablation technique in ours laboratories.

Tuning experimental parameters we demonstrate how to switch to different type of synthesized carbon nanomaterials, i.e., SWCNTs, CNOs, and graphene.

We show for the first time images of *SWCNTs in SEM, Z contrast, TEM, and EDX modes at the same sample location* leading to the identification of SWCNTs, catalyst grains and amorphous carbon.

Acknowledgements

This work was supported by Romanian Ministry of Education and by Executive Agency for Higher Education, Research, Development and Innovation Funding, under projects PCCA 2-nr. 166/2012 and ENIAC 04/2014.

Author details

Calin-Constantin Moise and Marius Enachescu*

*Address all correspondence to: marius.enachescu@upb.ro

Center for Surface Science and Nanotechnology, University Politehnica of Bucharest, Bucharest, Romania

References

[1] Kroto H.W., Heath J. R., O'Brien S. C., Curl R. F., Smalley R. E. (1985). C60: Buckminsterfullerene, *Nature*, 318, 162-163.

[2] Iijima S. (1991). Helical microtubules of graphitic carbon, *Nature*, 354, 56-58.

[3] Iijima S., Ichihashi T. (1993). Single-shell carbon nanotubes of 1-nm diameter, *Nature*, vol. 363, no. 6430, pp. 603–605.

[4] Geim A. K., Novoselov K. S. (2007). The rise of graphene, *Nature Materials*, 6, 183–191.

[5] Barbaro P., Bianchini C. (2009). Catalysis for Sustainable Energy Production, WILEY-VCH Verlag GmbH & Co. KGaA, pp. 123.

[6] Li J., Furuta T., Goto H., Ohashi T., Yip S. (2003). Theoretical evaluation of hydrogen storage capacity in pure carbon nanostructures, *Journal of Chemical Physics*, 119, 2376.

[7] Dillon A. C., Heben M. J.(2001). Hydrogen storage using carbon adsorbents: past, present and future, *Appl. Phys. A*, 72, 133–142.

[8] Liu C., Chen Y., Wu C.-Z., Xu S.-T., Cheng H.-M. (2010).Hydrogen storage in carbon nanotubes revisited, *Carbon* 48, 452–455.

[9] Besteman K., Lee J.-O., Wiertz F. G. M., Heering H. A., Dekker C. (2003). Enzyme-coated carbon nanotubes as single-molecule biosensors, *Nano Letters*, vol. 3, no. 6, pp. 727–730.

[10] Li J., Lu Y., Ye Q., Cinke M., Han J., Meyyappan M., (2003). Carbon nanotube sensors for gas and organic vapor detection, *Nano Letters*, vol. 3, no. 7, pp. 929–933.

[11] Uchihashi T., Choi N., Ashino M., Sugawara Y., Nishijima H., Akita S. (2000). Carbon-nanotubes tip for highly-reproducible imaging of deoxyribonucleic acid helical turns by noncontact atomic force microscopy, *Japanese Journal of Applied physics*, vol. 39, no. 8, pp. 667–889.

[12] Li J., Papadopoulos C., Xu J. (1999). Growing Y-junction carbon nanotubes, *Nature*, vol. 402, no. 6759, pp. 253–254.

[13] Dorobantu D., Bota P., Badea M., Boerasu I., Bojin D., Enachescu M., (June 2013). High quality and reliable carbon nano-structures used for 3rd generation of solar cells, *in Proceedings of the 37th Annual Congress of the American Romanian Academy of Arts and Sciences (ARA '37), Chisinau, Moldova.*

[14] Tomanek D. (2014) Guide Through the Nanocarbon Jungle Buckyballs, Nanotubes, Graphene, and Beyond, Michigan State University, Morgan & Claypool Publishers

[15] Krätschmer W., Lamb L. D., Fostiropoulos K., Huffman D. R. (1990). Solid C60: a new form of carbon, *Nature*, 347, 354.

[16] Guo T., Nikolaev P., Thess A., Colbert D. T., Smalley R. E. (1995). Catalytic growth of single-walled nanotubes by laser vaporization, *Chem. Phys. Lett.*, 243, 49–54.

[17] Scott C. D., Arepalli S., Nikolaev P., Smalley R. E. (2001). Growth mechanisms for single-wall carbon nanotubesin a laser-ablation process, *Appl. Phys. A*, 72, 573–580.

[18] Puretzky A. A., Geohegan D. B., Fan X., Pennycook S. J. (2000). Dynamics of single-wall carbon nanotube synthesis by laser vaporization, *Appl. Phys. A*, 70, 153–160.

[19] Puretzky A. A., Schittenhelm H., Fan X., Lance M. J., Allard L. F., Geohegan D. B. (2002). Investigations of single-wall carbon nanotube growth by time-restricted laser vaporization, *Phys. Rev. B,* 65, 245425.

[20] Nishide D., Kataura H., Suzuki S., Tsukagoshi K., Aoyagi Y., Achiba Y. (2003). High-yield production of single-wall carbon nanotubes in nitrogen gas, *Chemical Physics Letters*, vol. 372, no. 1–2, pp. 45–50.

[21] Al-Zanganawee J., Moise C., Katona A., Bojin D., Enachescu M. (2015). Characterization of single wall carbon nanotubes synthesized by KrF excimer laser ablation in nitrogen atmosphere, *Digest Journal of Nanomaterials and Biostructures*, vol. 10, no. 4, October–December, pp. 1119–1127.

[22] Al-zanganawee J., Katona A., Moise C., Bojin D., Enachescu M.(2015). Krypton gas for high quality single wall carbon nanotubes synthesis by KrF excimer laser ablation, *Journal of Nanomaterials,* Volume 2015, Article ID 909072, 7 pages http://dx.doi.org/10.1155/2015/909072 .

[23] Al-Zanganawee J., Mubarak T., Katona A., Moise C., Balan D., Dorobantu D., Bojin D., Enachescu M. (2016). Raman spectroscopy and morphology characterizations of SWCNTs synthesized by KrF excimer laser ablation under neon gas atmosphere, *Digest Journal of Nanomaterials and Biostructures*, vol. 11, no. 2, April–June, pp. 525–536.

[24] Moise C., Katona A., Dinescu D., Al-zanganawee J., Bojin D., Enachescu M.(2015). KrF excimer laser ablation in helium yields the highest amount of SWCNTs over other inert gases, *published in the Proceeding of The 39th American Romanian Academy of Arts and Sciences Congress National Institute of Nuclear Physics, Frascati, Rome, July 28-31, 2015.*

[25] Arepalli S., Nikolaev P., Holmes W., Bradley S. (2001). Production and measurements of individual single-wall nanotubes and small ropes of carbon, *Appl. Phys. Lett.*, 78, 1610.

[26] Holloway B. C., Eklund P. C., Smith M. W., Jordan K. C., Shinn M. (2010). April 6, *US Patent No. 7692116 B1.*

[27] Yahya N., Guan B. H., Hashim M. (2005). Development of pulsed laser deposition system for the formation of web-liked carbon nanotubes, *American Journal of Applied Sciences*, 11, 1509.

[28] Bota P. M., Dorobantu D., Boerasu I., Bojin D., Enachescu M. (2015). New laser ablation chamber for producing carbon nanomaterials using excimer laser, *Materials Research Innovations*, vol. 50, no. 1, pp. 33–39.

[29] Braidy N., El Khakani M. A., Botton G. A. (2002). Single-wall carbon nanotubes synthesis by means of UV laser vaporization, *Chemical Physics Letters*, vol. 354, no. 1-2, pp. 88–92.

[30] Kataura H., Kuzmazawa Y., Maniwa Y., Ohtuska Y., Sen R., Suzuki S., Achiba Y. (2000). Diameter control of single-walled carbon nanotubes, *Carbon*, 38, 1691-1697.

[31] Bota P. M., Dorobantu D., Boerasu I., Bojin D., Enachescu M. (2014). Synthesis of single-wall carbon nanotubes by excimerlaser ablation, *Surface Engineering and Applied Electrochemistry*, vol. 50, no. 4, pp. 11–15.

[32] Boerasu I., Enachescu M. (2013). Pulsed Laser Ablation Synthesis of Carbon Nano-Structures: Effect of Target Composition and Laser Ablation Condition on Their Yield and Morphology, Micro and Nanoengineering 2013 (http://www.nano-link.net/mne/volume22/5.pdf)

[33] Dorobantu D., Bota P. M., Boerasu I., Bojin D., Enachescu M. (2014). Pulse laser ablation system for carbon nano-onions fabrication, *Surface Engineering and Applied Electrochemistry*, 50 (5), 19–23.

[34] Pimenta M. A., Dresselhaus G., Dresselhaus M. S., Cancado L. G., Jorio A., Saito R. (2007). Studying disorder in graphite-based systems by Raman spectroscopy. *Physical Chemistry Chemical Physics*, 9, 1276–1290.